Journal of ELECTRONIC MATERIALS, Vol. 47, No. 5, 2018
https://doi.org/10.1007/s11664-018-6088-x

Impact of Ni Ion-Doping on Structural, Optoelectronic and Redox Properties of CeO_2 Nanoparticles

NAUSHAD AHMAD,[1] ANEES A. ANSARI,[2,4] JOSELITO P. LABIS,[2] and MANAWWER ALAM[3]

1.—Department of Chemistry, College of Sciences, King Saud University, Riyadh 11451, Kingdom of Saudi Arabia. 2.—King Abdullah Institute for Nanotechnology, King Saud University, Riyadh 11451, Kingdom of Saudi Arabia. 3.—Research Center, College of Sciences, King Saud University, Riyadh 11451, Kingdom of Saudi Arabia. 4.—e-mail: aneesaansari@gmail.com

We have investigated the influence of Ni doping on the physicochemical properties of CeO_2 synthesized by a co-precipitation process. As-prepared nanoparticles were characterized by x-ray diffraction pattern (XRD), transmission electron microscopy (TEM), energy dispersive x-ray analysis, thermal analysis, Fourier transform infrared spectra, optical absorption and temperature program reduction techniques. The observed results clearly demonstrate the impact of Ni ion concentration on the crystallinity, optoelectronic and reducibility of CeO_2 nanoparticles. XRD results show that the particle size was decreased after increasing the Ni ion-doping concentrations. TEM micrographs exhibited high aggregation in high Ni ion-doping concentration causing the smallest grain size of the materials. The band gap energies increased with decreasing particle size because of the higher oxygen-releasing capacity and stronger interaction between nickel and the CeO_2 matrix. The 7% mol Ni-doped CeO_2 exhibits low-temperature reduction. Because of excellent optoelectronic and redox properties, magnetically active Ni ion-doped CeO_2 nanoparticles can be used for electrochemical biosensors and solid oxide fuel cell catalysts can be potentially extended to other applications.

Key words: CeO_2 nanoparticles, nickel ion, band gap energy, optical absorption spectra, temperature program reduction

INTRODUCTION

Ceramic nanomaterials have wide technological applications due to their high thermal property, chemical stability, and excellent oxygen storage capacity.[1–4] Among these materials, cerium oxide (CeO_2) is attracting exceptional interest owing to its excellent physical and chemical aspects, which are remarkably different from other ceramic metal oxides.[2,3,5–7] CeO_2 is considered as the best catalyst support for DMR, CO oxidation and NOx reduction which provide not only good active metal dispersion throughout the support surface but also favor the carbonaceous deposit removal from the active sites.[8–13] The unique features are due to the distinct properties such as high oxygen storage capacity, redox process (couples of Ce^{4+}/Ce^{3+}), surface acidity and high thermal stability.[1,2,9,14,15] The rapid growth in the applications and the characterization of CeO_2-containing catalysts has been well documented.[10,12,15–19] Further, their microstructures are directly related to the surface-to-volume ratio, electrical and particle size which cause enhancement of conductivity, catalyst activation, and reaction kinetics when the microstructure was changed from micro- to nanocrystalline.[2,9,14,20,21] Nanocrystalline CeO_2 has opened up wide applications, such as electrolytes for solid oxide fuel cells, catalysts for the water gas shift reaction, abrasives for chemical–mechanical planarization, gas sensors, and hybrid solar cells.[9,10,12,13,15,18,19,22–24] Therefore, there is a great need to improve the redox property or oxygen

(Received June 10, 2017; accepted January 12, 2018; published online January 31, 2018)

storage capacity from the redesigning of the materials systems and thus improve the technology.[12,15,25–29] Among various methods, two feasible ones have been adopted in order to satisfy the above needs, namely, doping and modifying the preparation technique.[10,12,14,15,22,30]

Doping is an important and effective way to improve the electronic conductivity of ceramic metal oxide semiconductors. Various metal ions have been utilized for doping in cerium oxide nanomaterials,[9,10,12,13,21,23,25,27,30,31] which enhance the ionic conductivity of CeO_2 nanomaterials.[25,27–29] These transition and non-transition metal ion dopants interact at the interface of the CeO_2 crystal lattice, which enhances optical, redox and catalytic properties by changing energy band structure, mending the morphology and surface-to-volume ratio, and creating more active centers at the grain boundaries. Among them, NiO_x/CeO_2-based catalysts were found to be less expensive and showed wide applications. The remarkable performances of Ni-Ceria-based systems have been related to the ability of these oxides to show Ce^{3+}/Ce^{4+} oxidation states. The Ni^{2+} ion may have the tendency to enhance the grain boundary mobility of CeO_2 since its ionic size is much smaller than that of the matrix ion (i.e. Ce^{4+}). Here, the objective of the study is to find out the effects of nickel ion-doping on physiochemical characteristics such as crystal structure, crystallinity, morphology, thermal stability, and optoelectronic and redox behavior of CeO_2 nanoparticles.

EXPERIMENTAL

Materials

$Ce(NO_3)_36H_2O$ (99.99%BDH chemicals, UK), $Ni(NO_3)_23H_2O$ (99.9% E-Merck, Germany), $C_2H_6O_2$ (EG), C_2H_5OH, and NH_4OH were used directly as received without further purification. Milli-Q (Millipore, Bradford, USA) water was used for the synthesis and characterization of samples.

Synthesis of Nickel Ion-Doped CeO_2 Nanoparticles

Different concentrations of nickel ion-doped CeO_2 nanoparticles were prepared by a reflux-based co-precipitation method. For the preparation of nickel ion-doped CeO_2 nanoparticles, a freshly prepared 2 M aqueous solution of $Ce(NO_3)_36H_2O$ (different mol.% such as 99 mol.%, 97 mol.% and 93 mol.%) was poured into magnetically stirred 50 mL EG on a hot plate at 80°C. Then, a separately dissolved 2 M aqueous solution of $Ni(NO_3)_23H_2O$ (different mol.% such as 1 mol.%, 3 mol.% and 7 mol.%) was slowly injected into the mixed system and the whole solution was kept on a hot plate at 80°C with constant mechanical stirring for homogeneous mixing. After that, the properly mixed solution was hydrolyzed for 5–6 h at 100°C under reflux conditions. A minimum amount of ammonia solution was dropwise added to the reaction for precipitation. The light gray-colored precipitate was separated by centrifugation and washed with distilled water to remove unreacted reactants. For further characterization, the obtained products were dried in a muffle furnace at 400°C for 2 h. A similar procedure was applied for the synthesis of different concentrations of Ni ion-doped CeO_2 nanoparticles.

Characterization

X-ray diffraction patterns were prepared with a powder diffractometer (Rigaku, Dmax 2500) using *Cu K* radiation (λ = 1.5405 Å). Microscopic images were obtained from a field emission-transmission electron microscope (FE-TEM; JEM-2100F, JEOL, Japan) equipped with energy dispersive x-ray analysis (EDX) operating at an accelerating voltage of 200 kV. Stability and thermal properties were measured through thermogravimetric analysis (TGA/DTA; Mettler ToledoAnalytical CH-8603, Switzerland). Absorption spectra were recorded by a Carrying 60 (Agilent Technologies, USA) UV/Vis spectrophotometer within the UV/Vis range from 200 nm to 600 nm. Fourier transform infrared spectra were measured by a Vertex 80 (Brucker, USA) infrared spectrometer using the KBr pellet technique. A temperature-programmed reduction was performed on a chemisorption apparatus (Micromeritics AutoChem II-2920) equipped with a thermal conductivity detector. Briefly, about 50 mg of the sample was loaded in a U-shaped quartz tube (6 mm ID) with a flow rate of 20 mL/min of a mixture of 10% H_2/Ar gas. The temperature was ramped from ambient conditions to 500°C at a rate of 10°C/min. Water formed during the reduction was trapped by the cold trap. After the run, the TCD signal was plotted as a function of temperature.

RESULTS AND DISCUSSION

Crystallographic and Morphological Structure of Ni-Doped CeO_2 Nanoparticles

The phase purity, crystallinity and crystallographic structure of nickel-doped cerium oxide nanoparticles were analyzed by XRD, as shown in Fig. 1. The diffraction pattern consists of well-resolved peaks which have been indexed to the F*m3 m* space group in cubic symmetry. All samples exhibited six typical peaks corresponding to the (111), (200), (220), (311), (222), and (400) planes, providing clear evidence for the formation of the face-centered cubic fluorite structure of CeO_2, which is in good agreement with the value in the literature (JCPDS card No. 34–0394).[7,17,29] Any additional peaks related to NiO or salt were detected over the entire XRD range, and thus ruled out the formation of the secondary phase. The high purity of all samples demonstrates that nickel ions were homogeneously distributed inside the CeO_2 crystal lattice to form Ce-Ni-O solid solutions. Further, widening

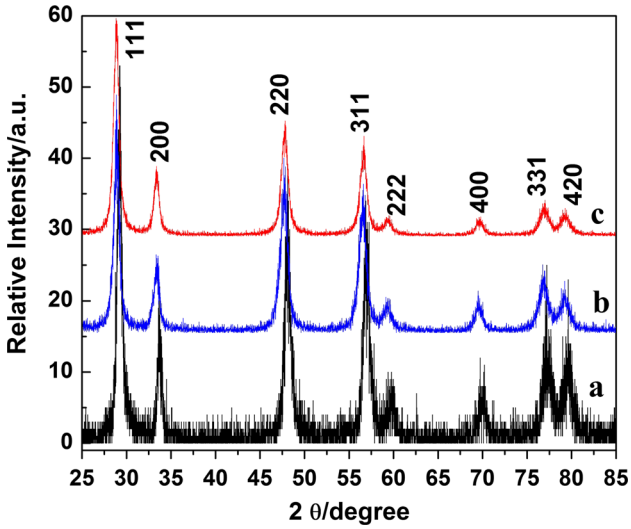

Fig. 1. X-ray diffraction patterns of (a) CeO_2:Ni1%, (b) CeO_2:Ni3%, and (c) CeO_2:Ni7% nanoparticles.

in the peak width shows that all the samples are prepared with primary small crystal particles. XRD peak intensity was relatively decreasing in the nickel-doped ceria samples. Additionally, insignificant shifting in XRD reflection lines of the solid Ce-O-Ni to longer 2θ angles corresponds to a shrinkage in the lattice parameters.[7,10] All diffraction peaks were broadened, clearly indicating the nano-crystalline behavior of the Ni-doped CeO_2 samples. The average crystallite size of all the samples was calculated from the peaks at the (111), (200), (220), and (311) planes using the Debye–Scherrer formulae. As observed from the XRD patterns, the particle size decreases from 15.4 to 12.6 nm with increasing Ni doping, indicating that Ni substitution hinders the growth of CeO_2 nanoparticles. Similar results have been reported in the literature on transition metal ion-doped CeO_2 nanoparticles.[31,32] The calculated lattice parameters from the XRD patterns for Ni-doped CeO_2 nanoparticles are 5.4224 for 1%, 5.4193 for 3% and 5.4101 Å for 7% doping. The decrease in lattice parameters with increasing concentration of Ni ions in the CeO_2 matrix could be related to the larger Ce^{4+} ions (0.101 nm) being replaced by smaller Ni^{2+} ions (0.069 nm), thus decreasing the lattice parameters, unit cell volume and crystallite size.[33]

Due to the limitation of the XRD measurements, high-resolution transmission electron microscopy (HR-TEM) measurements were used to obtain information about the shape, size, and presence of any secondary phase in the Ni-doped CeO_2 nanoparticles. Figure 2a–c represents the TEM micrographs of Ni-doped CeO_2 nanoparticles, from which it can be clearly seen that Ni-doped CeO_2 particles are in the nanometer range and have an almost spherical shape. As seen in Fig. 2a–c, the morphologies of all the prepared Ni-doped CeO_2 nanoparticles do not change much after increasing the doping concentration of nickel; however, their agglomeration and size distribution becomes higher due to the decrease in particle size. Similarly, Cavalcante et al.[34] observed that the PEG promote the aggregation of small particles or nucleation seeds on the surface through the lateral interaction of hydrogen bonding of water with the -OH groups of this polymer. It is observed that the average particle size decreases from 7.0 to 4.4 nm, which is consistent with the average particle size obtained from the peak broadening in XRD studies. Furthermore, to see any impurity phase in the doped samples, we performed SAED of the Ni-doped CeO_2 nanoparticles. The inset in Fig. 2a–c shows the SAED patterns of the Ni-doped CeO_2 nanoparticles. SAED patterns obtained by focusing the beam on the nanoparticles reveal the polycrystalline nature and phase purity of the Ni-doped CeO_2 nanoparticles. The lattice fringes are clearly visible with a spacing of 0.312 nm, which is in good agreement with the line spacing of the (111) planes of CeO_2. EDS was performed to further confirm the composition of the products. Figure 3a–c shows the EDX spectrograph of the Ni-doped CeO_2 samples. It shows the presence of different ions in the samples, which are assigned in the figure. The Ni^{3+} ion peak at $\sim$ 5.32 eV is very small as compared to other elements due to the presence of only a small amount, and its intensity gradually increases as the Ni ion concentration increases in the metal oxide nanoparticles. Appearances of strong Cu and C peaks in the middle of the EDX spectrum are from the carbon-coated copper grid.

The TGA profiles of the as-prepared Ni-doped CeO_2 nanoproducts from room temperature to 800°C are illustrated in Fig. 4. The three curves reveal remarkable thermal stability and similar decomposition patterns, which further confirms (by XRD analysis) the purity of the materials. All three curves are analogous in shape and show two-step thermal decay of the constituents. On the TGA curve, there is a slight decrease (up to 200°C) due to the crystalline and non-crystalline water molecules, which are attached to the nanoparticles in different coordination form. Additionally, in another decay step, a slow-moving mass loss (around 3%) is detected in all three curves between 200 and 800°C, which is due to the removal of small amounts of dangling bonds present on the surface of the nanoparticles.

Optical Properties

As can be seen in Fig. 5a–c, the curves are nearly the same. A diffuse band between 3200 cm^{-1} and 3650 cm^{-1} is observed, which is attributed to the stretching vibration of the physically associated water (O-H) molecules on the surface of the nanoparticles.[34–36] Another two bending vibrational bands of physically adsorbed water molecules are

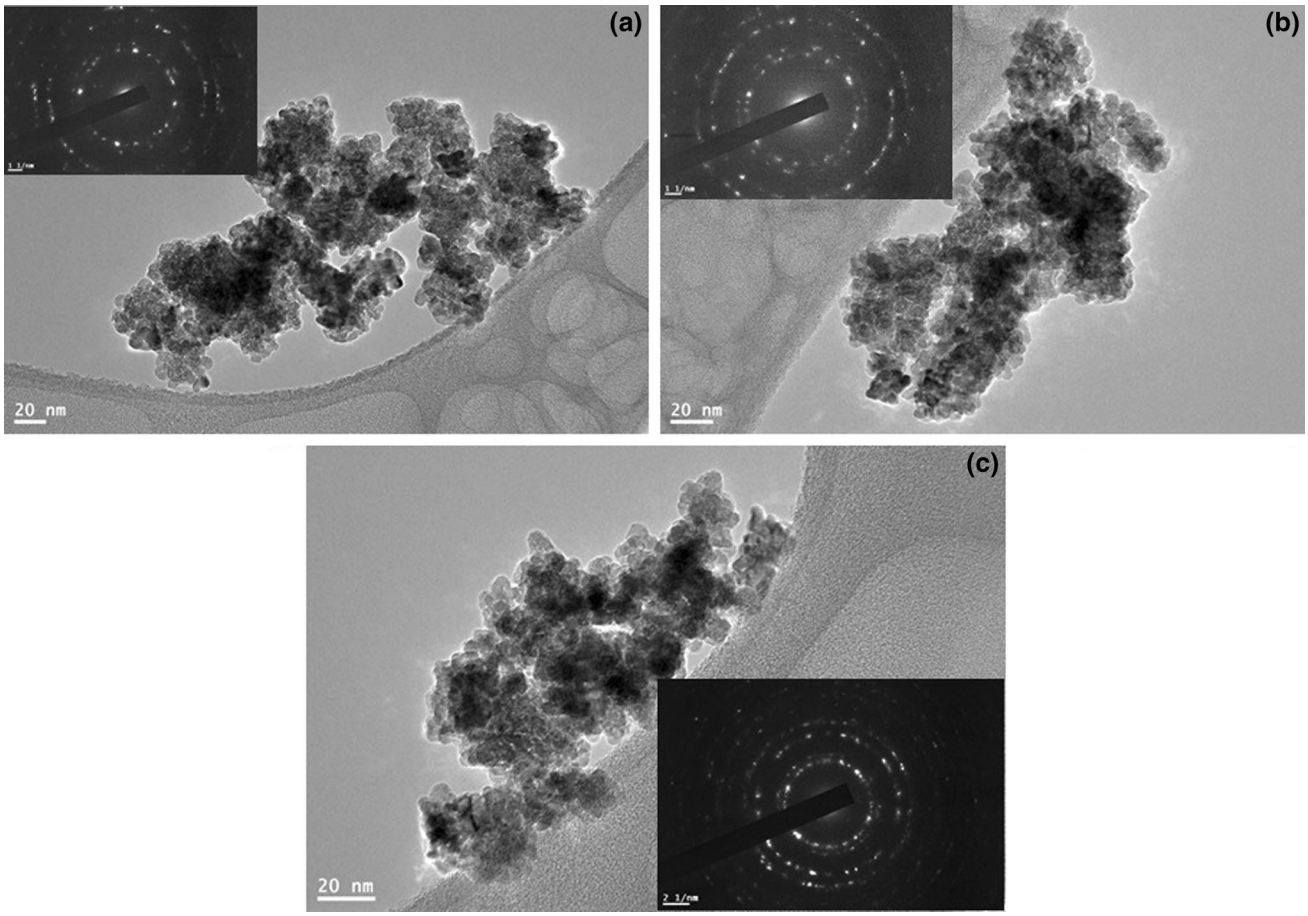

Fig. 2. FE-TEM micrographs of the as-prepared (a) CeO_2:Ni1%, (b) CeO_2:Ni3%, and (c) CeO_2:Ni7% nanoparticles. Inset the selected area electron diffraction pattern (SAED).

also observed at 1629 cm^{-1} and 1337 cm^{-1}. A strong peak also appears at about 483 cm^{-1}, which has been assigned to the Ce-O-Ni stretching band.[17,37,38]

The results of UV–Vis studies conducted on the Ni-doped CeO_2 nanoparticles reveal an absorption band in the wavelength region of 250–400 nm assigned to a charge transfer transition from the $O^{2-}(2p)$ to the Ce^{4+} $(4f)$ orbital in CeO_2.[35] Optical absorption spectra of the doped CeO_2 nanoparticles are similar in shape except for a slight hump observed in the 1-mol.% Ni-doped CeO_2 nanoparticle spectrum. In Fig. 6a–c, we did not observe a significant change in band shape, whereas the absorption edge is shifted toward a lower wavelength (blue shift) after increasing the Ni ion concentration. This clearly indicates the effect of Ni ions which are homogeneously distributed inside the cerium oxide lattice. Similar results have been reported by Thurber et al. in Ni-doped CeO_2 nanoparticles.[39] They observed that the band gap changed from 3.80 to 3.23 eV after doping of 4 mol.% Ni into the CeO_2 lattice. Thurber et al. ascribed that this change to additional structural changes caused by the incorporation of interstitial Ni, suggesting that the alteration in peak position is related to impurity defects (such as oxygen vacancies) or the contaminations caused by the assimilation of the Ni ions, as the imperfections and impurities could result in the formation of sublevels within the band gap.

It can be seen that the absorption edge obviously shifts towards the shorter wavelengths (blue shift). An estimate of the optical band gap, E_g, can be made by using the following equation for a semiconductor: $(\alpha h\nu)^n = \beta(h\nu - E_g)$, where $h\nu$ is the photon energy, α is the absorption coefficient, β is a constant relative to the material, and n is either two for a direct transition or ½ for an indirect transition. Figure 7 exhibits the curve of $(h)^2$ versus $h\nu$ for all three samples. The calculated energy band gaps for the 1 mol.%, 3 mol.% and 7 mol.% Ni ion-doped CeO_2 nanoparticles are found to be 2.28 eV, 2.56 eV and 2.68 eV, respectively (Fig. 7), and are thus lower in respect to the previously published reports and bulk counterpart (3.19 eV) due to a quantum confinement effect.[40] The lower E_g value of Ni-doped CeO_2

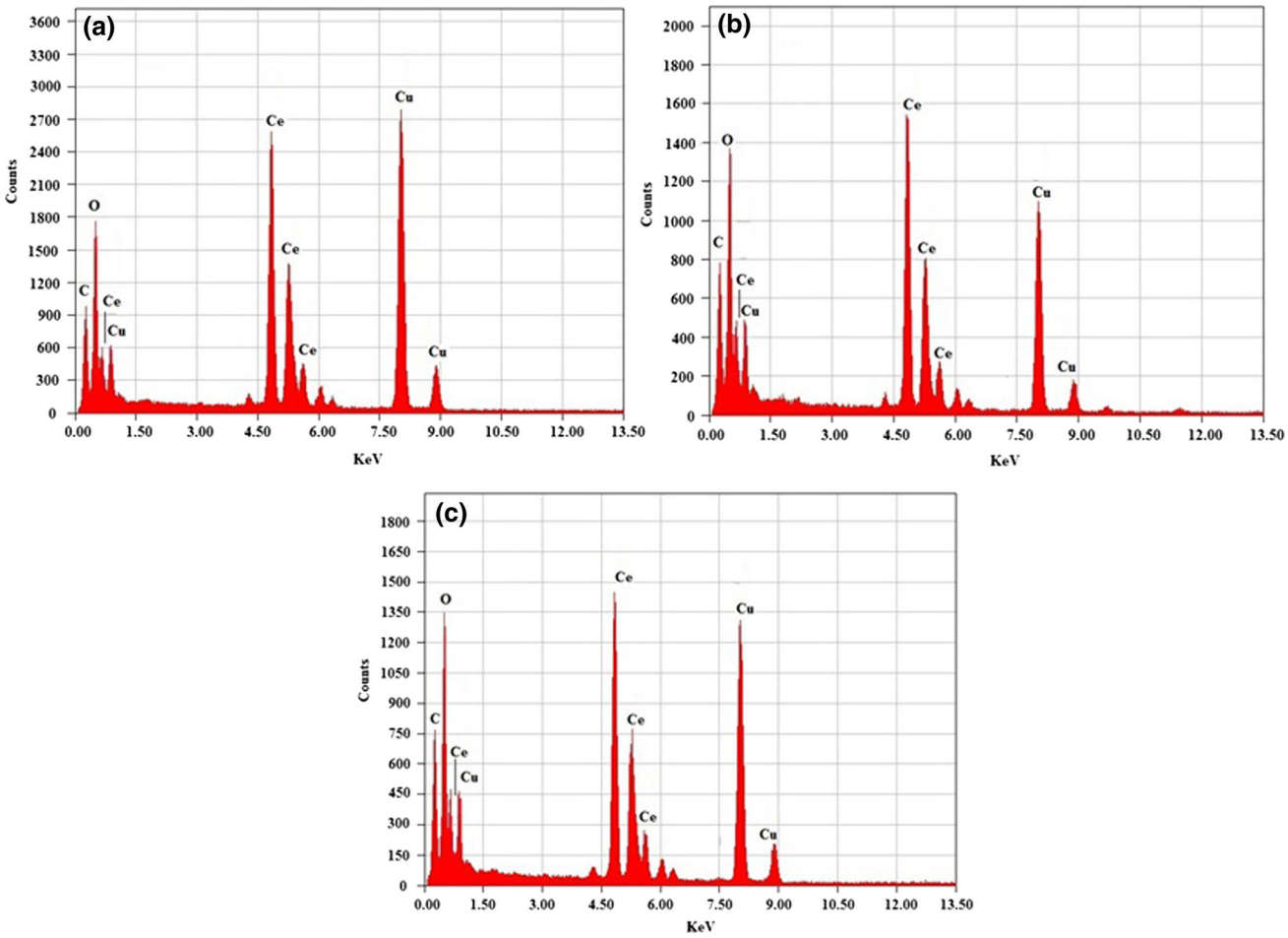

Fig. 3. EDX analysis of the as-prepared (a) CeO_2:Ni1%, (b) CeO_2:Ni3%, and (c) CeO_2:Ni7% nanoparticles.

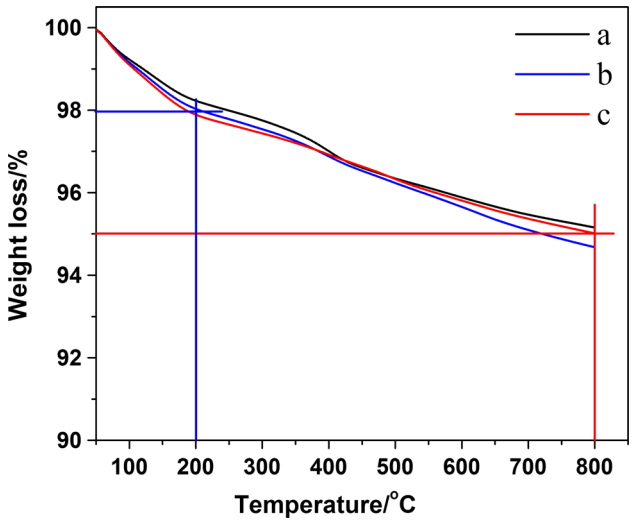

Fig. 4. Thermo-gravimetric analysis of (a) CeO_2:Ni1%, (b) CeO_2:-Ni3%, and (c) CeO_2:Ni7% nanoparticles.

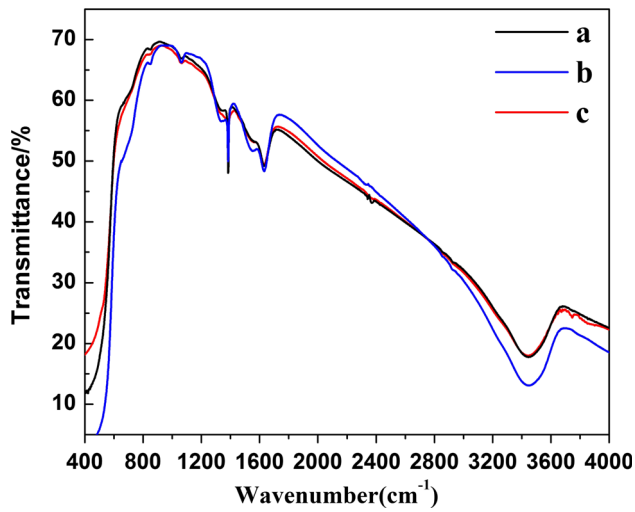

Fig. 5. FTIR spectra of (a) CeO_2:Ni1%, (b) CeO_2:Ni3%, and (c) CeO_2:Ni7% nanoparticles.

(2.68 eV) compared with that of pure CeO_2 (3.13 eV) is due to doping, as evidenced by their absorbance in the UV region. Doping with Ni ions creates oxygen vacancies and favors the formation of Ce^{3+} from Ce^{4+}. This increases the amount of Ce^{3+} states, resulting in the formation of localized energy states

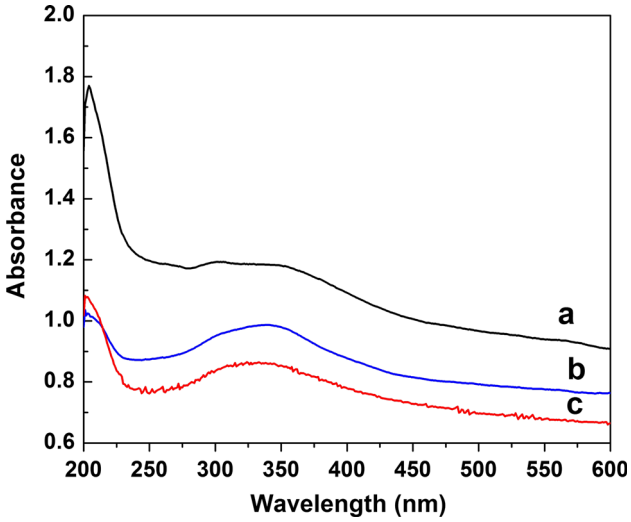

Fig. 6. UV–vis absorption spectra of (a) CeO_2:Ni1%, (b) CeO_2:Ni3%, and (c) CeO_2:Ni7% nanoparticles suspended in ethanol.

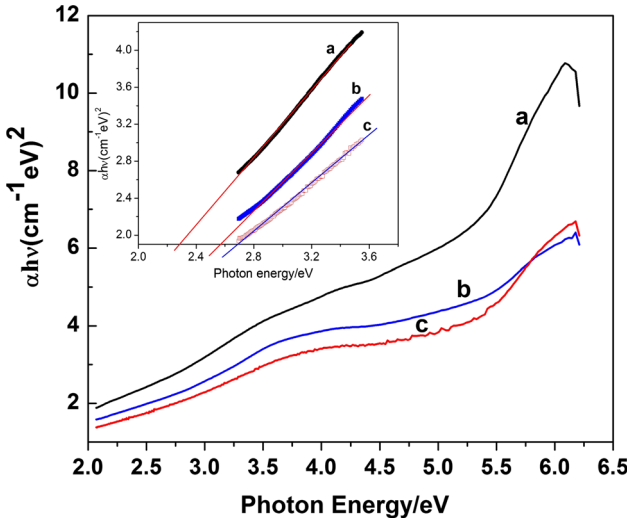

Fig. 7. Plot of $(\alpha h\nu)^2$ versus photon energy($h\nu$) of (a) CeO_2:Ni1%, (b) CeO_2:Ni3%, and (c) CeO_2:Ni7% nanoparticles.

that are closer to the conduction band and thereby decreasing the band gap.[41,42]

Temperature-Programmed Reduction Reaction (H_2-TPR)

In order to rationalize the doping effect of nickel ions on the reduction properties of CeO_2, temperature-programmed reduction studies were carried out. Figure 8 shows the temperature-programmed reduction profiles of the series Ni^{2+}-CeO_2 for different mol.%. The pure CeO_2 nanoparticles showed two bands: that at $\sim$ 124°C is attributed to the surface reduction of the ceria, while the second peak, at 403°C, is related to the bulk reduction of the ceria (Ce^{4+} to Ce^{3+}) (data not shown). The reduction

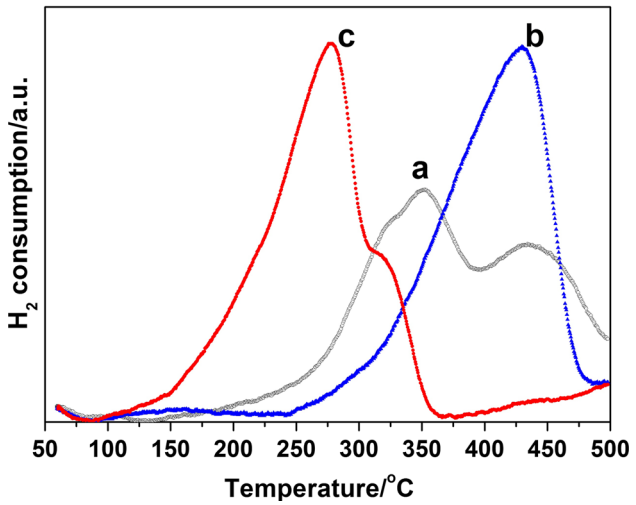

Fig. 8. Temperaturee-programmed reduction spectra of (a) CeO_2:Ni1%, (b) CeO_2:Ni3%, and (c) CeO_2:Ni7% nanoparticles.

profiles of the three catalysts show a singlet and doublet temperature of the maximum uptake of hydrogen (T_{max}) in the range 200–500°C, showing that reduction takes place in a singlet and stepwise. As seen in Fig. 8, 1-mol.% Ni-doped CeO_2 nanoparticles exhibit two reduction peaks, at about 350°C and 435°C, belonging to surface and bulk oxygen species reduction, indicating a stepwise reduction of Ni^{2+} to Ni^0. When the Ni ion concentration is increased, this doublet band merges in the singlet and the reduction band shifted to a lower temperature along with higher intensity, indicating the easy reducibility of the catalysts and higher hydrogen consummation. The calculated hydrogen consumption for 1.0%, 3.0% and 7.0% mol Ni-doped CeO_2 nanoparticles are 28 cm^3/g, 45 cm^3/g and 44.78 cm^3/g, respectively. Owing to the synergistic effect between Ni and CeO_2, the peak area is enhanced through the construction of a Ce-Ni-O solid solution, which can create O_2 deficiencies and structural alteration.[43–46] As more oxygen vacancies are formed, the surface oxygen concentrations of the doped CeO_2 samples are reduced; these observations are in accord with the XRD and energy band gap results. A similar behavior has been observed in the literature, and was assigned due to the surface reduction of the CeO_2 particles along with NiO reduction.[47,48] The temperature of the maximum uptake of hydrogen (T_{max}) increases in the order: 7 mol % < 3 mol % < 1 mol % Ni ion-CeO_2, showing that the reducibility of the catalysts increases in the reverse order, which plays an important role in determining the catalytic activity of the catalyst, particularly the dry reforming of methane.[43–48] This is consistent with the XRD results showing that increasing the Ni contents in the CeO_2 lattice leads to a gradual decrease in the crystalline size of the materials.

CONCLUSIONS

A polyol-assisted co-precipitation method was applied for the synthesis of different Ni ion-doped CeO_2 nanoparticles. The crystal structure and the thermal, optoelectronic and catalytic properties were systematically measured to investigate the effect of Ni ion-doping on the CeO_2 crystal lattice. The XRD results show that Ni-doped CeO_2 nanoparticles exhibit a single-phase nature with a cubic structure. The ring pattern as observed in SAED also confirms the single-phase nature of pure and Ni-doped CeO_2 nanoparticles. The structural parameters such as lattice parameters and particle size calculated from XRD and TEM were found to decrease with increasing the Ni ion doping. The band gap energies vary with the increase of Ni contents in the CeO_2 lattice. The introduction of Ni ions in the CeO_2 cubic fluorite structure enhanced the reduction of Ce^{3+} to Ce^{4+}, thereby the CeO_2 nanoparticles were reduced at low temperature ($\sim 275°C$). The 7-mol.% Ni ion-doped CeO_2 nanoparticles showed a higher reducing performance in comparison with the 3-mol.% Ni ion-doped CeO_2 nanoparticles due to an increase in the amount of Ni^{2+} at the surface. The higher redox activity of Ni ion-doped CeO_2 nanoparticles can be explained from the extent of Ce^{4+} reduction and the oxygen vacancies. Thus, this behavior is associated with a catalytic activity that indicates that this material may potentially be used for the development of electrochemical biosensors.

ACKNOWLEDGEMENT

The authors are grateful for financial support to King Saud University Deanship of Scientific Research, College of Sciences, Research Center.

REFERENCES

1. R.W. Tarnuzzer, J. Colon, S. Patil, and S. Seal, *Nano Lett.* 5, 2573 (2005).
2. S. Patil, S. Seal, Y. Guo, A. Schulte, and J. Norwood, *Appl. Phys. Lett.* 88, 243110 (2006).
3. F. Zhang, S.W. Chan, J.E. Spanier, E. Apak, Q. Jin, R.D. Robinson, and I.P. Herman, *Appl. Phys. Lett.* 80, 127 (2002).
4. C.G. Levi, J.Y. Yang, B.J. Dalgleish, F.W. Zok, and A.G. Evans, *J. Am. Ceram. Soc.* 81, 2077 (1998).
5. S. Tsunekawa, S. Ito, and Y. Kawazoe, *Appl. Phys. Lett.* 85, 3845 (2004).
6. S. Patil, S.C. Kuiry, and S. Seal, *Proc. R. Soc. Math. Phys.* 460, 3569 (2004).
7. S. Deshpande, S. Patil, S.V.N.T. Kuchibhatla, and S. Seal, *Appl. Phys. Lett.* 87, 133113 (2005).
8. X.Y. Zhang, J.J. Wei, H.X. Yang, X.F. Liu, W. Liu, C. Zhang, and Y.Z. Yang, *Eur. J. Inorg. Chem.* 2013, 4443 (2013).
9. R.H. Gao, D.S. Zhang, P. Maitarad, L.Y. Shi, T. Rungrotmongkol, H.R. Li, J.P. Zhang, and W.G. Cao, *J. Phys. Chem. C* 117, 10502 (2013).
10. J.C. Zhang, J.X. Guo, W. Liu, S.P. Wang, A.R. Xie, X.F. Liu, J. Wang, and Y.Z. Yang, *Eur J. Inorg. Chem.* 6, 969 (2015).
11. W.P. Shan, F.D. Liu, H. He, X.Y. Shi, and C.B. Zhang, *Chem. Commun.* 47, 8046 (2011).
12. J.Y. Luo, M. Meng, J.S. Yao, X.G. Li, Y.Q. Zha, X. Wang, and T.Y. Zhang, *Appl. Catal. B Environ.* 87, 92 (2009).
13. G. Jacobs, L. Williams, U. Graham, G.A. Thomas, D.E. Sparks, and B.H. Davis, *Appl. Catal. Gener.* 252, 107 (2003).
14. X.F. Wan, D. Goberman, L.L. Shaw, G.S. Yi, and G.M. Chow, *Appl. Phys. Lett.* 96, 3371678 (2010).
15. A. Hornes, G. Munuera, A. Fuerte, M.J. Escudero, L. Daza, and A. Martinez-Arias, *J. Power Sources* 196, 4218 (2011).
16. A. Kaushik, P.R. Solanki, A.A. Ansari, S. Ahmad, and B.D. Malhotra, *Nanotechnology* 20, 055105 (2009).
17. A.A. Ansari, P.R. Solanki, and B.D. Malhotra, *Appl. Phys. Lett.* 92, 263901 (2008).
18. D.S. Zhang, Y.L. Qian, L.Y. Shi, H.L. Mai, R.H. Gao, J.P. Zhang, W.J. Yu, and W.G. Cao, *Catal. Commun.* 26, 164 (2012).
19. G. Jacobs, L. Williams, U. Graham, D. Sparks, and B.H. Davis, *J. Phys. Chem. B* 107, 10398 (2003).
20. N. Thovhogi, A. Diallo, A. Gurib-Fakim, and M. Maaza, *J. Alloy. Compd.* 647, 392 (2015).
21. S. Khamlich, B.D. Ngom, C.K. Kotsedi, K. Bouziane, E. Manikandan, and M. Maaza, *Surf. Rev. Lett.* 21, 1450001 (2014).
22. S. Mahammadunnisa, P.M.K. Reddy, N. Lingaiah, and C. Subrahmanyam, *Catal. Sci. Technol.* 3, 730 (2013).
23. Q. Fu, W.L. Deng, H. Saltsburg, and M. Flytzani-Stephanopoulos, *Appl. Catal. B Environ.* 56, 57 (2005).
24. S.X. Cai, D.S. Zhang, L. Zhang, L. Huang, H.R. Li, R.H. Gao, L.Y. Shi, and J.P. Zhang, *Catal. Sci. Technol.* 4, 93 (2014).
25. T.Y. Yu, J. Zeng, B. Lim, and Y.N. Xia, *Adv. Mater.* 22, 5188 (2010).
26. M. Balaguer, C. Solis, S. Roitsch, and J.M. Serra, *Dalton T* 43, 4305 (2014).
27. L. Liao, H.X. Mai, Q. Yuan, H.B. Lu, J.C. Li, C. Liu, C.H. Yan, Z.X. Shen, and T. Yu, *J. Phys. Chem. C* 112, 9061 (2008).
28. S. Banerjee, P.S. Devi, D. Topwal, S. Mandal, and K. Menon, *Adv. Funct. Mater.* 17, 2847 (2007).
29. C. Laberty-Robert, J.W. Long, K.A. Pettigrew, R.M. Stroud, and D.R. Rolison, *Adv. Mater.* 19, 1734 (2007).
30. H.J. Lang, K. Kunstler, and G. Tomandl, *Solid State Ionics* 157, 189 (2003).
31. Z.P. Qu, F.L. Yu, X.D. Zhang, Y. Wang, and J.S. Gao, *Chem. Eng. J.* 229, 522 (2013).
32. M. Li, Z.G. Liu, Y.H. Hu, Z.X. Shi, and H.Q. Li, *Colloid Surface A* 301, 153 (2007).
33. D. Channei, B. Inceesungvorn, N. Wetchakun, S. Ukritnukun, A. Nattestad, J. Chen, and S. Phanichphant, *Sci. Rep. Uk* 4, 5757 (2014).
34. V.S. Marques, L.S. Cavalcante, J.C. Sczancoski, A.F.P. Alcantara, M.O. Orlandi, E. Moraes, E. Longo, J.A. Varela, M.S. Li, and M.R.M.C. Santos, *Cryst. Growth Des.* 10, 4752 (2010).
35. A.A. Ansari, S.P. Singh, and B.D. Malhotra, *J. Alloy. Compd.* 509, 262 (2011).
36. A.A. Ansari, A. Kaushik, P.R. Solanki, and B.D. Malhotra, *Electrochem. Commun.* 10, 1246 (2008).
37. A.A. Ansari, P.R. Solanki, and B.D. Malhotra, *Sensor Lett.* 7, 64 (2009).
38. A.A. Ansari, S.P. Singh, N. Singh, and B.D. Malhotra, *Spectrochim Acta A* 86, 432 (2012).
39. A. Thurber, K.M. Reddy, V. Shutthanandan, M.H. Engelhard, C. Wang, J. Hays, and A. Punnoose, *Phys. Rev. B* 76, 165435 (2007).
40. T. Masui, K. Fujiwara, K. Machida, G. Adachi, T. Sakata, and H. Mori, *Chem. Mater.* 9, 2197 (1997).
41. B. Tatar, E.D. Sam, K. Kutlu, and M. Urgen, *J. Mater. Sci.* 43, 5102 (2008).
42. P. Patsalas, S. Logothetidis, L. Sygellou, and S. Kennou, *Phys. Rev. B* 68, 035104 (2003).
43. C.N. Xian, S.F. Wang, C.W. Sun, H. Li, S.W. Chan, and L.Q. Chen, *Chin. J. Catal.* 34, 305 (2013).
44. P. Maitarad, J. Han, D.S. Zhang, L.Y. Shi, S. Namuangruk, and T. Rungrotmongkol, *J. Phys. Chem. C* 118, 9612 (2014).

45. L. Meng, A.P. Jia, J.Q. Lu, L.F. Luo, W.X. Huang, and M.F. Luo, *J. Phys. Chem. C* 115, 19789 (2011).
46. B.M. Reddy, L. Katta, and G. Thrimurthulu, *Chem. Mater.* 22, 467 (2010).
47. H.Q. Zhu, Z.F. Qin, W.J. Shan, W.J. Shen, and J.G. Wang, *J. Catal.* 225, 267 (2004).
48. H.C. Yao and Y.F.Y. Yao, *J. Catal.* 86, 254 (1984).